

## EFFECT OF NANOSIZE SiO<sub>2</sub> PARTICLES ADDED INTO ELECTROLYTE ON THE COMPOSITION AND MORPHOLOGY OF OXIDE LAYERS FORMED IN ALLOY AK6M2 UNDER MICROARC OXIDIZING

M. M. Krishtal,<sup>1</sup> P. V. Ivashin,<sup>1</sup> I. S. Yasnikov,<sup>1</sup> and A. V. Polunin<sup>1</sup>

Translated from *Metallovedenie i Termicheskaya Obrabotka Metallov*, No. 7, pp. 62 – 69, July, 2015.

Oxide layers formed on AK6M2 aluminum-silicon alloy by microarc oxidizing (MO) are studied. The chemical and phase compositions and the morphology of the layers deposited from a base-composition electrolyte with different contents of added SiO<sub>2</sub> powder are determined. It is shown that high-temperature phases form in the oxide layer at a specific concentration of SiO<sub>2</sub> nanoparticles. This indicates elevation of the effective temperature in the zone of synthesis of the oxide layers in the process of MO. The addition of nanosize particles of SiO<sub>2</sub> into the electrolyte influences positively the operating characteristics of the formed oxide layer.

**Key words:** microarc (plasma-electrolytic) oxidizing, nanoparticles, silica, silumin, oxide layer, phase composition, elemental composition, morphology.

### INTRODUCTION

The development of microarc (plasma-electrolytic) oxidizing (MAO or PAO) is aimed at improving the quality of coatings and raising the rate and controllability of the process. This is especially important for aluminum-silicon alloys used widely in different branches of industry. One of the most important factors influencing the process of oxidizing of aluminum alloys is the presence of silicon and silicon-containing compounds. For example, it has been shown in [1, 2] that the distribution of silicon in the matrix of the alloy affects considerably the quality of the oxide layer formed by MAO on aluminum-silicon alloys. The influence of silicon-containing compounds dissolved in the electrolyte on the process of MAO of aluminum alloys and on the properties of the obtained oxide layers is studied in [3–7]. However, the mechanism of MAO has not been determined in full and its study continues [8–11].

One of the methods to improve the characteristics of oxide layers formed by MAO is filling of the pores and flaws of the oxide layer with fine particles from the electrolyte [12, 13]. Such modification of the oxide layer is commonly aimed at raising the strength, lowering the friction factor, etc. by choosing an appropriate material of the particles filling the flaws. The use of nanosize particles for modifying oxide

layers presents special interest [14]. The mechanism of the interaction between nanoparticles and liquid or plasma is a subject of recent research. The results of [15–17] allow us to expect unsuspected effects of interaction of nanoparticles, the electric discharge plasma and the oxide layer forming under MAO. Specifically, we may expect that nanoparticles should affect the occurrence of the microarc discharge in its different phases and the kinetics of oxidation under MAO in addition to filling the oxide layer flaws. Since the MAO process is affected considerably by silicon and its compounds, silicon-containing nanoparticles should be especially interesting. In our earlier experiments described in [5–7] we established that the introduction of SiO<sub>2</sub> particles into the electrolyte under MAO changes the thermal conductivity and the mechanical properties of the oxide layer. The aim of the present work was to determine the influence of silica particles in the electrolyte on the chemical and phase composition and on the morphology of the oxide layer in the process of microarc oxidizing of aluminum-silicon alloy AK6M2 chosen as an example.

### METHODS OF STUDY

Oxide layers were deposited by microarc oxidizing on flat specimens of silumin AK6M2. The alloy had the following chemical composition (in wt.%): 5.9 Si, 2.0 Cu, 0.4 Mg, 0.1 Mn, 0.4 Fe, 0.05 Zn, 0.1 Ti, 0.05 Ni, the remainder Al.

<sup>1</sup> Tolyatti State University, Tolyatti, Russia (e-mail: krishtal@tltsu.ru).

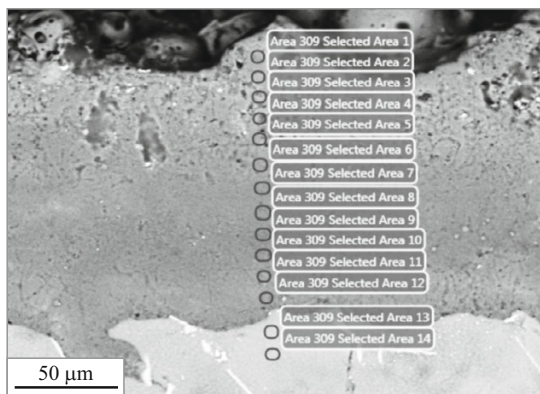


**Fig. 1.** Regions scanned by x-ray spectrum microanalysis of a transverse microsection of oxide layer on alloy AK6M2.

The specimens were  $20 \times 50 \times 5$  mm in size. Before synthesizing an oxide layer the specimens were subjected to a T6 heat treatment, i.e., homogenizing annealing at  $515 \pm 5^\circ\text{C}$  for 8 h, quenching from  $515 \pm 5^\circ\text{C}$  in water heated to  $80^\circ\text{C}$ , and aging at  $235 \pm 5^\circ\text{C}$  for 4 h. This mode of treatment is optimum for formation of a quality oxide layer on siluminis by the method of MAO [18].

Microarc oxidizing was performed in an alkaline-silicate solution based on distilled water. The solution contained:

- 4 g/liter NaOH (GOST 4328–77, grade ChDA);
- 12 g/liter liquid sodium glass Na<sub>2</sub>SiO<sub>3</sub> (with density  $\rho = 1.45 \times 10^3$  kg/m<sup>3</sup>, silica modulus  $m = 3$ , GOST 13078–81);
- 8 g/liter Na<sub>2</sub>HPO<sub>4</sub> · 12H<sub>2</sub>O (GOST 4172–76).

The process of MAO was conducted for 150 min in an anode-cathode regime from an ac source with a frequency of 50 Hz. An anode-to-cathode ratio of 1.0–1.15 was maintained constant during the whole of the process. The anode forming voltage was (1) 400 V for 30 min, (2) 500 V for 30 min, (3) 600 V for 60 min, and (4) 550 V for 30 min. The initial current density was about 0.25 A/cm<sup>2</sup>.

The variable factor in the tests was the addition of silica nanoparticles (grade “Tarkosil” [19]) in an amount of up to 7 g/liter. The particles were x-ray amorphous and had an average fineness of 20 nm. The preliminary XRD analysis of the nanosize powder of SiO<sub>2</sub> did not show the presence of any crystal phases in it.

We studied the phase and chemical composition, the structure, and the morphology of the surface of the oxide layers.

The x-ray diffraction analysis of the oxide layers was performed with the help of a Shimadzu Maxima XRD-7000 diffractometer with filtered copper  $K_\alpha$  radiation.

To determine the chemical elements in the oxide layers we used a Carl Zeiss Sigma 02-09 scanning electron microscope with a EDAX module for x-ray spectrum microanalysis and plotted the map of the distribution of elements in the oxide layer. The qualitative analysis of the elements was performed after plotting the maps of their distribution in

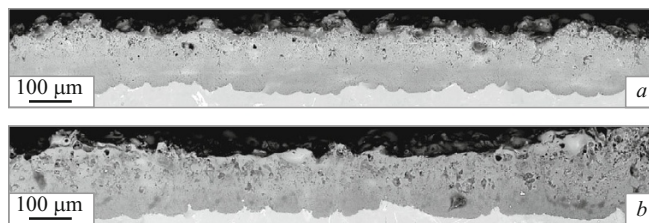


**Fig. 2.** Structure of oxide layer (transverse section) obtained on alloy AK6M2 in base electrolyte (a) and in an electrolyte with 7 g/liter nanoparticles of SiO<sub>2</sub> (b).

transverse microsections to visualize the special features of the distribution.

Quantitative estimates were obtained by analyzing the elements in the following manner.

1. We chose zones with a size of 1–2 μm in the cross section for scanning and obtained the spectra from them (Fig. 1).

2. In each zone we evaluated the content of the following elements: O, Na, Mg, Al, and Si.

3. We plotted the linear distribution of the elements in the cross section of the layer in weight percent according to the position of the scanned zones.

The morphology of the surface of the oxide layers was studied with the help of an Olympus LEXT OLS4000 confocal laser microscope. The resolution of the scanning was 0.625 μm; the scanning area was  $640 \times 640$  μm; the error of the determination of the profile coordinates did not exceed 2%. In addition, we studied the morphology of the surface using a Carl Zeiss Sigma 02-09 scanning electron microscope.

The porosity and the flaws of the coatings were also studied on transverse microsections with the help of a scanning electron microscope with an AsB detector.

## RESULTS

### Microstructure of the Oxide Layer

The structure of an oxide layer in a cross section is presented in the panoramic photographs obtained with the help of a scanning electron microscope (Fig. 2). It can be seen that the layer consists of two zones with substantially different structure. The surface (external) zone that takes 40–50% of the thickness of the layer has a well manifested inhomogeneous porous structure. The internal zone has lower porosity and is visually more homogeneous. It can be seen that the thickness of the external layer is somewhat larger for the oxide layer obtained with the addition of SiO<sub>2</sub> nanoparticles into the electrolyte. For the subsequent study we assumed that the thickness of the external zone took 40% of the thickness of the entire oxide layer.

### Content of Elements in the Oxide Layer

Figure 3 presents maps of the distribution of elements in oxide layers obtained in different electrolytes. Figure 4

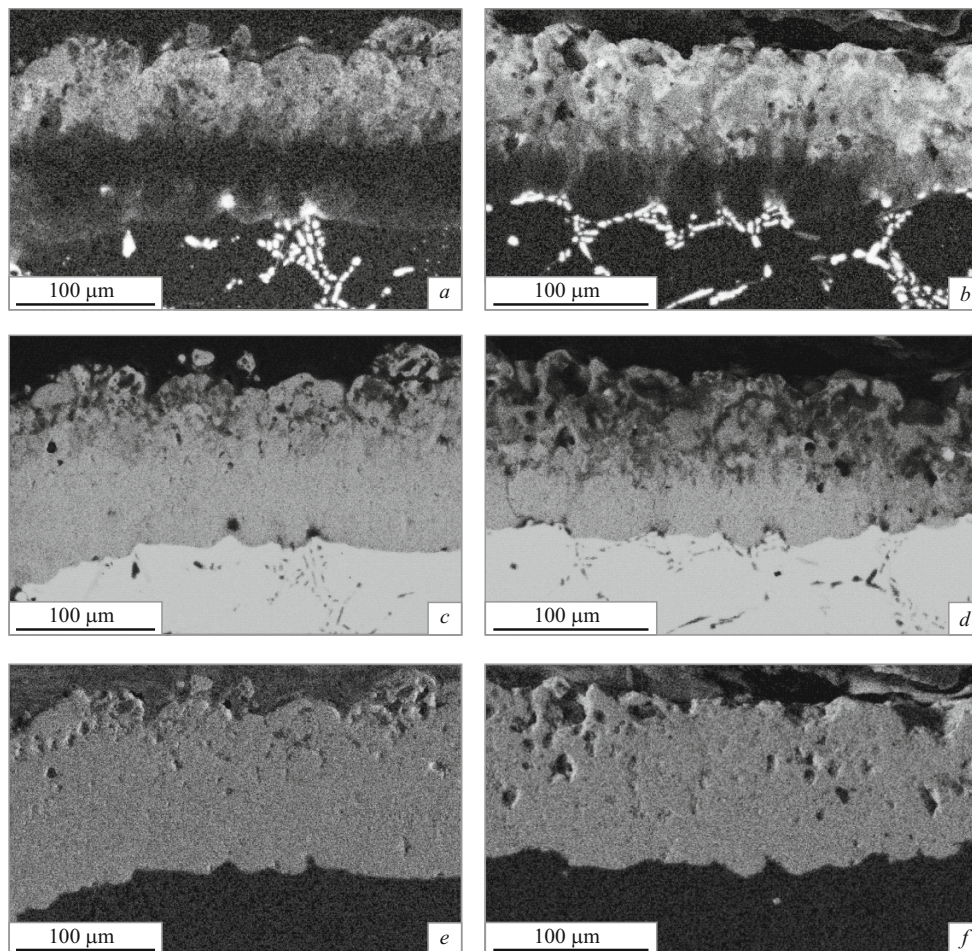


**Fig. 3.** Maps of distribution of silicon (*a, b*), aluminum (*c, d*) and oxygen (*e, f*) in oxide layers formed on alloy AK6M2 in base electrolyte (*a, c, e*) and an electrolyte with 7 g/liter  $\text{SiO}_2$  nanoparticles (*b, d, f*) (dark-background images).

shows the variation of their concentration over the thickness of the layers.

We can observe more uniform distribution of silicon in the loose part of the oxide layer, where its concentration is higher (Fig. 3*a* and *b*) than in the internal zone that touches the substrate. This will be confirmed by the results of the quantitative analysis presented below. The nonuniformity of the distribution silicon in the internal part of the oxide layer is also “inherited” from the structure of the oxidized alloy, which agrees with the data of [1].

We established (Fig. 3*c* and *d*) that the content of aluminum in the external zone of the layer is less uniformly distributed than in the dense internal zone. This is especially vivid for the layer formed with the addition of nanoparticles into the electrolyte (Fig. 3*d*).

In contrast to silicon and aluminum, oxygen (Fig. 3*e* and *f*) is distributed over the oxide layer uniformly, and the kind of its distribution is virtually independent of the presence of nanoparticles in the electrolyte.

The results of the analysis of the linear distribution of elements in a cross section of the oxide layer are presented in

Fig. 4. It can be seen that the fraction of oxygen remains virtually unchanged over the whole of the layer, while the growth in the content of silicon is compensated by decrease in the content of aluminum. The growth in the silicon content and the decrease in the concentration of aluminum in the external part of the oxide layer upon the addition of  $\text{SiO}_2$  nanoparticles into the electrolyte is more considerable than in the case of the use of the base electrolyte. It should also be noted that the concentrations of aluminum and silicon are constant in the internal dense and external loose zones of the layer but vary intensely in the transition regions. This matches the results of the known works [10, 11], which also report growth in the proportion of silicon in the external part of the layer. Thus, the concentration of silicon in the oxide layer varies depending on the scanning coordinate. For example, the distribution of silicon (with concentration of at most 4%) in the part of the oxide layer joining the substrate (which takes 20 – 30% of the thickness of the layer) is virtually uniform. In the external part of the layer (about 40% of the thickness) the concentration of silicon is also constant. In what follows, we will estimate the concentration of elements

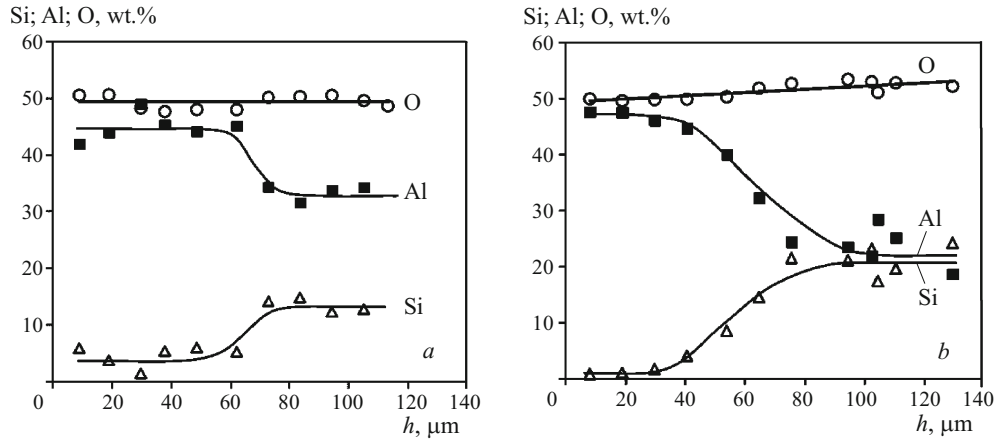


**Fig. 4.** Distribution of aluminum, silicon and oxygen over the thickness of oxide layers on alloy AK6M2 formed in base electrolyte (*a*) and in an electrolyte with 7 g/liter nanoparticles (*h* is the distance from the “alloy – oxide layer” interface in the direction to the surface of the layer).

in the external part of the layer as an arithmetic mean of four-five values corresponding to the scanning zones in the more loose external zone of the layer, where the concentration of silicon and aluminum is about constant.

Since the thickness of the layers formed in different electrolytes somewhat differs, we plotted the concentration of the elements as a function of relative coordinates for visual representation of the changes in the distribution of elements in cross section of the oxide layer. These coordinates were obtained by dividing the coordinates of the scanned zone by the thickness of the layer at the scanned place. The zero corresponds to the “substrate – oxide layer” interface.

Figure 5 presents the distribution of silicon and sodium in cross section of the oxide layer for specimens obtained in electrolytes with different contents of SiO<sub>2</sub> nanoparticles. It can be seen from Fig. 5a that the concentration of silicon in the external zone of the oxide layer increases upon growth in the content of SiO<sub>2</sub> nanopowder in the electrolyte.

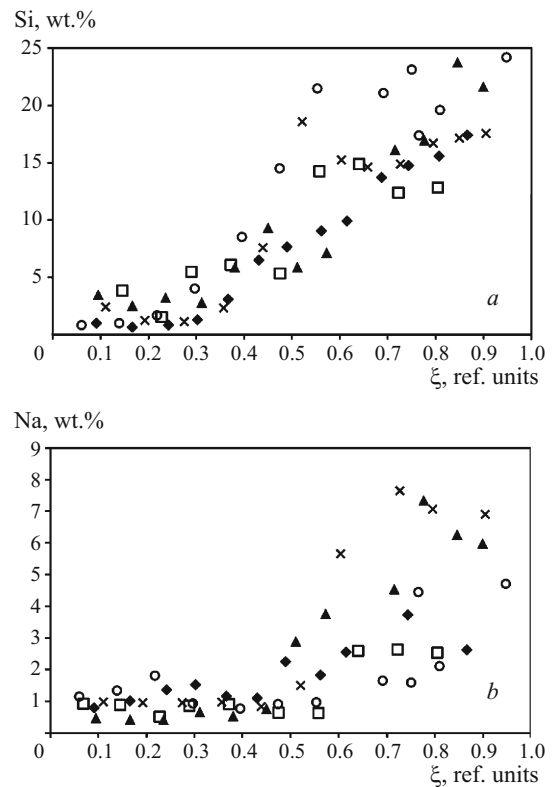
In contrast to silicon, the distribution of sodium in the oxide layer (Fig. 5b) has a manifested maximum after the addition of 5 g/liter SiO<sub>2</sub> nanoparticles into the electrolyte.

Figure 6a presents the concentrations of sodium and silicon in the external zone of the oxide layer as a function of the content of SiO<sub>2</sub> nanoparticles in the electrolyte.

### Phase Composition of Oxide Layers

Phase analysis of the oxide layers obtained in the standard electrolyte has shown the presence of a rhombic ( $\alpha$ ) and cubic ( $\gamma$ ) phases of aluminum oxide and mullite (a mineral of the class of silicates with nonconstant chemical composition from  $3\text{Al}_2\text{O}_3 \cdot 2\text{SiO}_2$  to  $2\text{Al}_2\text{O}_3 \cdot \text{SiO}_2$ ). The proportion of different phases in the oxide layer depends nonlinearly on the concentration of x-ray amorphous SiO<sub>2</sub> nanoparticles in the electrolyte (Fig. 6b). The content of the Al<sub>2</sub>O<sub>3</sub>  $\alpha$ -phase in the oxide layer is maximum when nanosize silica is added into the electrolyte in the content of 3 g/liter. In this case the con-

tent of the Al<sub>2</sub>O<sub>3</sub>  $\gamma$ -phase and mullite is minimum. In addition, when SiO<sub>2</sub> nanoparticles are added into the electrolyte in an amount of 1 – 5 g/liter, a new SiO<sub>2</sub> phase (tridymite) not typical for the oxide layer synthesized in the base electro-



**Fig. 5.** Distribution of silicon (*a*) and sodium (*b*) over the thickness of oxide layer on alloy AK6M2 ( $\xi = h_i/h_1$ , where  $h_i$  is the distance from the “alloy – oxide layer” interface to the center of the zone of spectrum accumulation and  $h_1$  is the total thickness of the oxide layer). The concentration of nanoparticles in the electrolyte is: □) 0 g/liter; ◆) 1 g/liter; ▲) 3 g/liter; ×) 5 g/liter; ○) 7 g/liter.

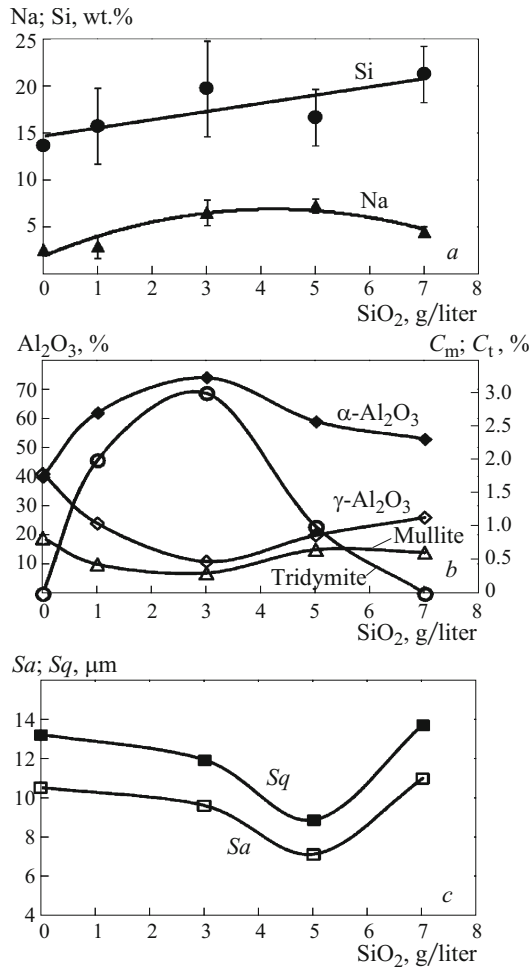


**Fig. 6.** Content elements in the external part of oxide layer (a), phase composition (b) and surface roughness of the layer (c) on alloy AK6M2 as a function of the addition of SiO<sub>2</sub> nanopowder into the electrolyte: C<sub>t</sub>, C<sub>m</sub>) contents of tridymite and mullite, respectively.

lyte forms in the oxide layer. It can be seen from Fig. 6b that the curves have well manifested extrema, i.e., maximums for the high-temperature phases (α-Al<sub>2</sub>O<sub>3</sub> and tridymite) and minimums for the low-temperature phases (mullite and γ-Al<sub>2</sub>O<sub>3</sub>) at 3–5 g/liter silica nanopowder in the electrolyte.

### Morphology of the Surface of Oxide Layers

The results of the study with the help of an Olympus Lext confocal scanning laser microscope have shown that the morphology of the surface of the oxide layers formed in electrolytes with different contents of SiO<sub>2</sub> nanopowder differ considerably. We used the ISO 25178 Standard for estimating the surface roughness of the whole of the scanned area in order to compare the microprofiles of the studied oxide layers. We determined the mean square (Sq) and mean arithmetic (Sa) values of the height of the surface microprofile. The results of the estimation of the roughness of the oxide layers are presented in Fig. 6c. It can be seen that the influence of

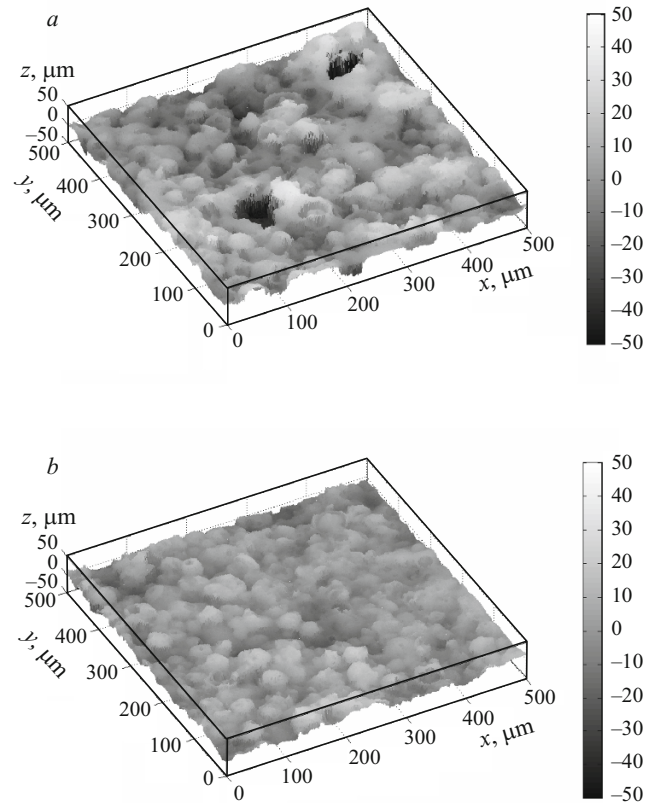


**Fig. 7.** Regions of microprofile of the surface of oxide layer on alloy AK6M2 formed in base electrolyte (a) and in an electrolyte with an additive of 5 g/liter SiO<sub>2</sub> nanoparticles (b).

the addition of SiO<sub>2</sub> nanopowder into the electrolyte is non-linear; the roughness is minimum at the concentration of 5 g/liter SiO<sub>2</sub> nanopowder in the electrolyte. Figure 7 presents images of surface regions of oxide layers. It can be seen that the microprofile of the surface becomes smoother upon the addition of nanoparticles into the electrolyte.

Further analysis of the morphology of the surface of oxide layers obtained at different contents of SiO<sub>2</sub> nanoparticles in the electrolyte was performed with the help of a scanning electron microscope. It can be seen from Fig. 8 that the surfaces of the specimens differ substantially depending on the addition of SiO<sub>2</sub> into the electrolyte. The surface of the oxide layers formed at different concentrations of SiO<sub>2</sub> nanoparticles in the electrolyte contains smooth fused regions (Fig. 8a), bubbles with traces of gas emission from them (Fig. 8b), and broken bubbles with finer structural components units of micron in size (Fig. 8 and Fig. 9a).

In addition, peculiar structural elements in the form of curved “cords” units of micron in diameter and tens of micron in length have been discovered on the surface of the oxide layer formed in the electrolyte with an additive of 3 g/liter (Fig. 9b) nanopowder. The results of the x-ray spectrum microanalysis across a “cord” (line AB in Fig. 9b) are presented in Fig. 10. The main elements on the surface of the “cord” are aluminum, oxygen and silicon. The fraction of si-

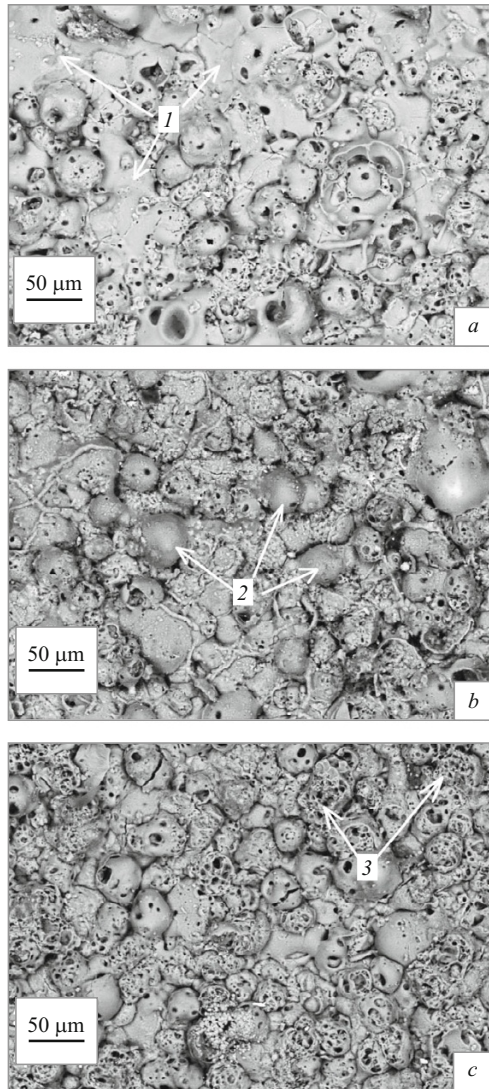


**Fig. 8.** Structure of the surface of oxide layer formed on alloy AK6M2 under oxidizing with different additives of SiO<sub>2</sub> nanopowder into the electrolyte: *a*) 0 g/liter; *b*) 3 g/liter; *c*) 5 g/liter; 1) fused regions; 2) frozen bubbles with traces of gas emission; 3) broken bubbles.

liron is about 50%; that of aluminum exceeds slightly the background level, i.e., the material of the “cord” should be a modification of SiO<sub>2</sub> or an aluminum silicate of a variable composition.

## DISCUSSION

The tendency to elevation of the concentration of silicon in the external part of the layer upon the addition of nanoparticles into the electrolyte (Figs. 5*a* and 6*a*) seems to be a result of their presence in the structure of the oxide layer. However, other facts show a positive action of the addition of SiO<sub>2</sub> nanoparticles into the electrolyte, specifically, on the ignition and burning of the microarc discharge.

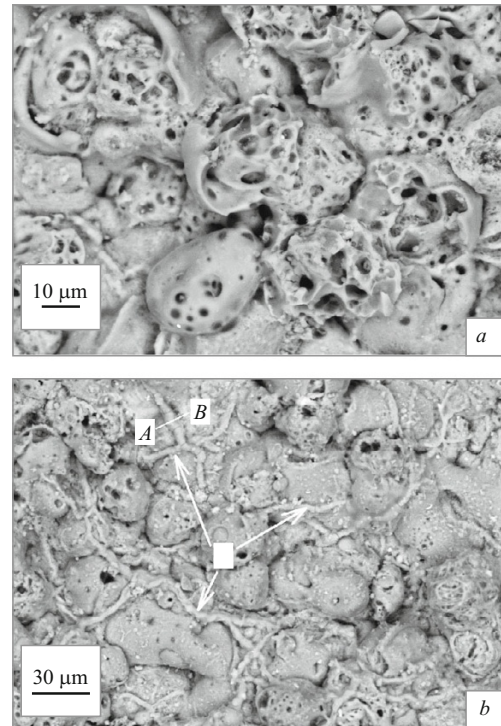


**Fig. 9.** Magnified structure of the surface of oxide layer: *a*) loose structure of fractured bubbles; *b*) “cords” (indicated by the arrows; *AB*) line of scanning in the x-ray spectrum analysis of the “cords”).

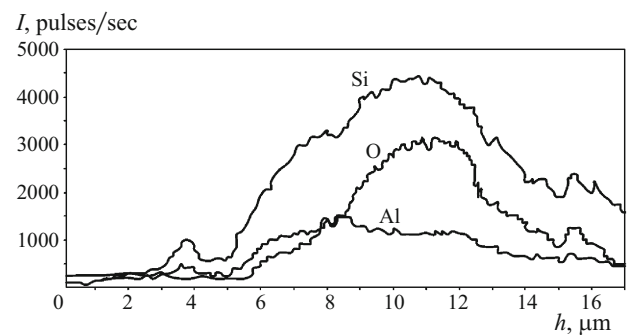


**Fig. 10.** Results of x-ray spectrum microanalysis of a “cord” over line *AB* (see Fig. 9*b*).

The nonlinear variation of the concentration of sodium in the oxide layer with maximum in the case of 3 g/liter SiO<sub>2</sub> nanoparticles in the electrolyte is an indication of changes in the MAO process, because the content of sodium in the electrolyte remains unchanged. In other words, the addition of 3 g/liter nanoparticles of SiO<sub>2</sub> into the electrolyte accelerates the process of mass transfer of sodium from the electrolyte into the oxide layer.

The facts of the appearance of a new SiO<sub>2</sub> phase (tridymite) formed at a temperature of 950 – 1500°C [20], which is not typical for oxide layers formed in the base electrolyte, and of the growth in the content of the α-Al<sub>2</sub>O<sub>3</sub> phase ap-

pearing above 900°C [21] show that the temperature in the reaction of zone of MAO increases upon the addition of nanoparticles into the electrolyte.

New structural elements of the surface morphology (“cords”) appearing upon the addition of 3 g/liter SiO<sub>2</sub> nanoparticles into the electrolyte reflect changes in the process. The same addition causes the greatest change in the phase composition of the oxide layer.

Considerable leveling of the microtexture of the surface upon the addition of nanoparticles into the electrolyte (up to 5 g/liter) also indicates growth of the temperature on the surface of the specimen.

Thus, it can be assumed that the addition of SiO<sub>2</sub> nanoparticles into the electrolyte not only causes their transfer into the oxide layer but also affects the microarc discharge. The nonlinearity of the effect of the concentration of SiO<sub>2</sub> nanoparticles in the electrolyte on the chemical and phase composition and morphology of the surface (Fig. 6) implies competition of two oppositely directed mechanisms. It is possible that the dielectric [22] nanoparticles of SiO<sub>2</sub> hinder the electric breakdown between the electrolyte and the specimen. However, getting into the high-temperature zone of the already burning microarc discharge and splitting into charged particles, the nanoparticles of SiO<sub>2</sub> stabilize the burning of the microarcs. When the optimum concentration of SiO<sub>2</sub> nanoparticles in the electrolyte is exceeded, the conditions for the appearance of microarc discharges are worsened due to the inhibitory dielectric action of the nanoparticles.

## CONCLUSIONS

1. Addition of nanosize powder of silica into the electrolyte used for microarc oxidizing of aluminum-silicon alloy AK6M2 affects substantially the chemical and phase composition and the morphology of the obtained oxide layers.

2. The presence of 1 – 5 g/liter SiO<sub>2</sub> nanoparticles in the electrolyte produces a new SiO<sub>2</sub> phase (tridymite) in the oxide layer; the temperature of formation of this phase is 950°C. The content of this phase varies nonlinearly depending on the concentration of nanoparticles in the electrolyte and is maximum at 3 g/liter. At the same concentration of SiO<sub>2</sub> nanoparticles in the electrolyte we observe a maximum content of high-temperature  $\alpha$ -Al<sub>2</sub>O<sub>3</sub> phase and a minimum content of  $\gamma$ -Al<sub>2</sub>O<sub>3</sub> and mullite, which should promote substantial improvement of the mechanical and heat-insulating characteristics of the oxide layer.

3. In oxidizing with an addition of SiO<sub>2</sub> nanoparticles into the electrolyte the content of silicon increases and the content of sodium in the external part of the oxide layer varies nonlinearly. The sodium concentration in the oxide layer has a maximum at 3 g/liter nanopowder of silica in the electrolyte.

4. Introduction of 3 – 5 g/liter SiO<sub>2</sub> nanoparticles into the electrolyte lowers the roughness of the oxide layer by

more than 30% and produces new components in the morphology of the surface. For example, the addition of 5 g/liter SiO<sub>2</sub> has reduced the roughness of the surface Sa from 10.5 to 7  $\mu$ m. When the concentration of SiO<sub>2</sub> nanoparticles in the electrolyte is raised to 7 g/liter, the roughness increases to Sa = 1  $\mu$ m.

*The work has been performed with support of State Research Engineering Assignment (Project 887).*

## REFERENCES

1. M. M. Krishtal and M. O. Ryumkin, “Effect of the initial structure of Al – Si alloys on the properties of oxide layers obtained by the method of microarc oxidizing and on deceleration of growth of the oxide layer by silicon particles,” *Materialovedenie*, No. 12, 50 – 61 (2008).
2. M. M. Krishtal, “Effect the structure of aluminum-silicon alloys on the process of formation and characteristics of oxide layer under microarc oxidizing,” *Metall. Term. Obrab. Met.*, No. 9, 20 – 25 (2004).
3. I. V. Suminov, P. N. Belkin, A. V. Épel’feld, et al., *Plasma-Electrolytic Modification of the Surface of Metals and Alloys* [in Russian], Tekhnosfera (2011), Vol. 2, 512 p.
4. A. V. Tokarev, “Electrophysical characteristics of coatings on aluminum deposited by the method of microarc oxidizing,” *Vestn. KRSU*, **12**(10), 106 – 110 (2012).
5. M. M. Krishtal, P. V. Ivashin, I. A. Rastegaev, et al., “Effect of alloying of the electrolyte with nanosize silica on the tribological characteristics of oxide layers formed on an aluminum-silicon alloy by microarc oxidizing,” *Vektor Nauki TGU*, No. 1, 48 – 52 (2014).
6. A. V. Polunin, P. V. Ivashin, I. A. Rastegaev et al., “A study of the wear resistance of oxide layers formed on silumin AK9PCh by microarc oxidizing in an electrolyte modified with silica nanoparticles,” *Deform. Razrush. Mater.*, No. 2, 21 – 25 (2015).
7. M. M. Krishtal, P. V. Ivashin, D. A. Pavlov, and A. V. Polunin, “About the heat conduction of oxide coatings deposited by the method of microarc oxidizing on silumin AK9PCh,” *Vektor Nauki TGU*, No. 4(22), 169 – 172 (2012).
8. V. Dehnavi, B. Luan, D. Shoosmith, et al., “Effect of duty cycle and applied current frequency on plasma electrolytic oxidation (PEO) coating growth behavior,” *Surf. Coat. Technol.*, **226**, 100 – 107 (2013).
9. F. Monfori, A. Berkani, E. Matykina, et al., “Development of anodic coatings on aluminum under sparking conditions in silicate electrolyte,” *Corros. Sci.*, **49**(2)[672], 672 – 693 (2007).
10. F. Monfori, E. Matykina, A. Berkani, et al., “Species separation during coating growth on aluminum by spark anodizing,” *Surf. Coat. Technol.*, **201**(21), 8671 – 8676 (2007).
11. K. Wang, Joo Kim Young, Hayashi Yasunori, et al., “Ceramic coatings on 6061 Al alloys by plasma electrolytic oxidation under different AC voltages,” *J. Ceram. Proc. Res.*, **10**(4), 562 – 566 (2009).
12. A. N. Bolotov, D. A. Zorenko, and V. V. Novikov, *A Method for Electrolytic Deposition of Antifriction Coating on Aluminum and Its Alloys*, RF Patent 2220233 [in Russian].
13. F. Jin, P. K. Chu, H. Tong, and J. Zhao, “Improvement of surface porosity and properties of alumina films by incorporation of Fe micrograins in micro-arc oxidation,” *Appl. Surf. Sci.*, **253**, 863 – 868 (2006).

14. E. Matykina, R. Arrabal, P. Skeldon, and G. E. Thompson, "Incorporation of zirconia nanoparticles into coatings formed on aluminum by AC plasma electrolytic oxidation," *J. Appl. Electrochem.*, **38**(10), 1375 – 1383 (2008).
15. V. Ya. Rudyak, A. A. Belkin, and E. A. Tomilina, "The force acting on a nanoparticle in liquid," *Pis'ma Zh. Teor. Fiz.*, **34**(2), 69 – 74 (2008).
16. Yu. N. Kul'chin, O. B. Vitrik, V. P. Dzyuba, and N. P. Kraeva, "Relaxation of the speed of nonequilibrium nanoparticles in liquid," *Pis'ma Zh. Teor. Fiz.*, **37**(12), 58 – 66 (2011).
17. Yu. V. Martynenko, M. Yu. Nagel, and M. A. Orlov, "Nanoparticle in plasma," *Fizika Plazmy*, **35**(6), 542 – 546 (2009).
18. M. M. Krishtal, "A wear-resistant coating for aluminum-silicon alloys using microarc oxidation and an application to an aluminum cylinder block," in: *SAE Paper 2002-01-0626* (2002), pp. 152 – 162.
19. S. P. Bardakhanov, V. I. Lysenko, A. V. Nomoev, and D. Yu. Trufanov, "A ceramics for nanopowders and its properties," *Steklo Keram.*, No. 12, 10 – 13 (2008).
20. V. Swamy, K. Suxena Surendra, et al., "A thermodynamic assessment of silica phase diagram," *J. Geophys. Res.: Solid Earth (1978 – 2012)*, **99**(B6), 11,787 – 11,794, 10 June (1994).
21. G. D. Chukin, "The structure of alumina and of catalysts for hydrodesulfurization," in: *Reaction Mechanisms* [in Russian], OOO "Printa," Moscow (2010), 288 p.
22. S. P. Bardakhanov, A. P. Zav'yalov, K. V. Zobov, et al., "A study of electrophysical properties of nanosize powders of silica, alumina and nickel," *Vestn. NGU, Ser. Fiz.*, **4**(1), 75 – 79 (2009).